Journal of the Meteorological Society of Japan

## EARLY ONLINE RELEASE



The DOI for this manuscript is
DOI:10.2151/jmsj. 2018-002
J-STAGE Advance published date: September 29, 2017
The final manuscript after publication will replace the preliminary version at the above DOI once it is available.

# Extension of a multisensor satellite radiance-based evaluation for cloud system resolving models

**Woosub ROH**

*Atmosphere and Ocean Research Institute*
*The University of Tokyo, Chiba, Japan*

**and**

**Masaki Satoh**

*Atmosphere and Ocean Research Institute*
*The University of Tokyo, Chiba, Japan*

May 29, 2017

-----------------------------------
1) Corresponding author: Woosub Roh, the University of Tokyo, 5-1-5, Kashiwanoha, Kashiwa-shi, 277-8568, JAPAN.
Email: ws-roh@aori.u-tokyo.ac.jp
Tel: +81- 4-7136-4371
Fax: +81-4-7136-4375

## Abstract

As an alternative approach to the previous multisensor satellite evaluation method of cloud system resolving models, a method is presented using combined infrared and microwave channels for precipitation clouds in cloud system resolving models over the ocean. This method determines characteristics of cloud-top temperatures and ice scatterings for clouds using infrared 11-μm and microwave high frequencies (89.0 GHz) brightness temperatures (TBs). The threshold of the TB at low frequencies (18.7 GHz) is also used to identify precipitation regions. This method extends the previous approach via the wider swath of the passive microwave sensor and sensitivities to ice clouds compared to the previous Tropical Rainfall Measuring Mission (TRMM)-based analysis method using the narrower coverage of the Precipitation Radar.

The numerical results of the non-hydrostatic icosahedral atmospheric model (NICAM) with two cloud microphysics schemes are evaluated over the tropical open ocean using this method. The intensities of the scatterings in the two simulations at 89.0 GHz are different due to the parameterizations of the snow and graupel size distributions. A bimodal size distribution of the snow improved the underestimation of the TBs at 89.0 GHz. These results have a similar structure to the joint histograms of cloud-top temperatures and precipitation-top heights in the previous method: the overestimated intensity of scattering and the frequencies of high precipitation-top heights above 12 km in the control experiment. We find that the change in the snow size distribution in the cloud microphysics scheme can lead to better agreements of simulated TBs at 89.0 GHz with observations. We further investigate impacts of non-spherical assumptions for snow using a satellite simulator. The effect of a non-spherical shape of snow in the radiative transfer model causes a smaller change of TBs at 89.0 GHz compared to the difference between the TBs of the two simulations without non-spherical assumptions.

**Keywords** Cloud system resolving models; a satellite simulator; evaluations of cloud microphysics; passive microwave satellites

## Introduction

Recently, various methods have been proposed to evaluate and improve the cloud microphysics schemes of cloud system resolving models (CSRMs) using satellite data. One method is a radiance-based evaluation to avoid making assumptions about the microphysical properties between retrieval algorithms and CSRMs using a satellite simulator (Masunaga 2010; Hashino 2013; Matsui 2014). Using the Tropical Rainfall Measuring Mission (TRMM) and a satellite simulator (Matsui et al. 2009, 2016), Roh and Satoh (2014) (hereafter RS14) improved cloud properties over the tropical Pacific Ocean simulated by the non-hydrostatic icosahedral atmospheric model (NICAM; Tomita and Satoh 2004; Satoh et al. 2008; Satoh et al. 2014), such as the precipitation cloud statistics in terms of the cloud-top temperatures (CTT) and the precipitation-top heights (PTHs), and the contoured frequency altitude diagrams of the radar reflectivities. RS14 improved their single-moment bulk microphysics scheme using the preferred size distributions from multiple sensitivity tests to reproduce realistic cloud statistics, accumulated precipitation, and outgoing longwave radiation (OLR). Roh et al. (2017) expanded RS14 to evaluate global simulations with 3.5-km mesh horizontal resolutions and found improvements in various types of clouds over the global domain in comparison with the TRMM and CloudSat observations.

RS14 and Roh et al. (2017) used the method proposed by Matsui et al. (2009) known as the TRMM Triple-Sensor Three-Step Evaluation Framework (T3EF). This method is innovative because multisensor observations are used to evaluate the CSRMs using satellite simulators. However, because TRMM precipitation radar (PR) has a relatively narrow 250-km swath, the applicability of T3EF is limited to sampling volumes for relatively short-term and small domain simulations.

Passive microwave observations in satellites have been used to estimate quantitative precipitation. The low frequencies (<20 GHz) of microwave sensors have a direct physical relationship between the path integrated water content of the rain and radiances over the ocean. For high frequencies (>80 GHz), the radiances are depressed by the scattering of large ice particles such as snow, graupel, and hail. The microwave observations enable us to obtain precipitation information, including ice clouds, particularly in deep convective systems.

Previous studies have used microwave observations to evaluate the precipitation systems of CSRMs (Eito and Aonashi (2009); Matsui et al. 2009; Han et al. 2010). For example, Eito and Aonashi (2009) found fairly good agreement between the simulated and observed brightness temperatures (TBs) at 18.7 GHz but a stronger intensity of scattering at high frequencies (36.5 GHz and 89.0 GHz) than in the observations, using the Japan Meteorological Agency non-hydrostatic model (JMA-NHM) and observations of the Advanced Microwave Scanning Radiometer for Earth Observing System (AMSR-E).

In this study, we introduce a method of radiance-based evaluation using microwave and infrared channels and satellite simulators over the ocean. This method is an extension of

T3EF and has two advantages: (1) a wider range of coverage compared to TRMM PR and (2) ice cloud information. We evaluate the numerical results from NICAM using two cloud microphysics schemes over the tropical open ocean and investigate the impact of the snow and graupel size distributions.

## Numerical experimental design and observational data

NICAM is a global non-hydrostatic model that can be used as a regional model by transforming the horizontal grid system to focus on a region of interest (the stretched NICAM; Tomita 2008b). Simulations using the stretched version of NICAM are evaluated following the case of RS14. The analysis domain is over the tropical central Pacific region between latitudes 10°S and 10°N and longitudes 170°E and 170°W. Mesoscale convective systems (MCSs) are dominant in this case and the convective band occurred at approximately 5°N latitude over the analysis domain. The minimum of the horizontal grid spacing of the domain is 2.4 km at the central point of the domain and most of the grid sizes are less than 5 km. We focus on the period from 06 UTC January 1 to 06 UTC January 6 2007. Two microphysics schemes are used and evaluated: the original NICAM Single-Moment Water (NSW6) scheme (hereafter, CON; Tomita, 2008a) and the modified NSW6 scheme (hereafter, MODI) following Roh et al. (2017).

The microwave data are from AMSR-E on the Aqua satellite. AMSR-E has a 1450-km swath at the surface and measures microwave emissions at six separate frequencies

(6.925 GHz, 10.65 GHz, 18.7 GHz, 23.8 GHz, 36.5 GHz, and 89.0 GHz). The dual-polarized microwave radiometer operates at the six separate frequencies for both the vertical and horizontal polarizations. The polarization differences between the vertically polarized and horizontally polarized brightness temperatures at 18.9 GHz (D19; Liu and Curry 1998; Eito and Aonashi 2009) and the polarization corrected 89-GHz brightness temperatures (PCT89, Spencer et al. 1989) are derived from AMSR-E L2A (Ashcroft and Wentz 2013), which has a spatial resolution of 39 km at 18.7 GHz and 12 km at 89.0 GHz. D19 is representative of the atmospheric emission from liquid water itself and is close to 0 in the strong emission areas (Liu and Curry 1998). PCT89 is calculated in order to reduce an impact of the inhomogeneity of surface emissivity (Kidd 1998)

The CTTs are taken from the 11-μm infrared channels with 0.04° resolution and 30 minutes interval on the Multifunction Transport Satellite (MTSAT) geostationary satellite. The CTTs are matched with AMSR-E data having the closest time. We sampled observation data from the same period of simulations.

To compare our results with RS14, joint histograms of the CTT and PTH are constructed (Masunaga and Kummerow 2006; Matsui et al. 2009) following RS14. The PTH is identified as the highest altitude of the layer above a PR reflectivity of 20 dBZ. The infrared 11-μm TBs for the CTTs from the TRMM 1B01 product and the 13.8 GHz reflectivity and orbital precipitation from TRMM 2A25 are used for the PTH.

We used two satellite simulators to compare the radiances of the observational data with those of the NICAM data: the first, satellite simulator developed at Florida University (hereafter the Liu simulator; Liu 1998; Liu 2008) for the 18.7 GHz and 89.0 GHz microwave TBs of AMSR-E, and the second, Satellite Data Simulator Unit (SDSU; Masunaga et al. 2010) version 2.1.4 for the 11-μm TBs and radar reflectivities at 13.8 GHz. The four-stream radiative transfer model is used and the non-spherical database for the ice clouds is implemented in the Liu simulator. The Gaussian beam convolution is applied to the two microwave channels in the Liu simulator following Masunaga and Kummerow (2005) to reduce the uncertainty from the antenna pattern of passive microwave sensors. The extinction and scattering properties of the hydrometeors are calculated based on the Mie calculation in the two simulators. The effective dielectric constant of snow and graupel is calculated based on the Maxwell-Garnett approach (Maxwell-Garnett 1904), which was generalized by Bohren and Battan (1982). We assumed the snow density ($\rho_s$) like $\rho_s = 100$ kg $m^{-3}$ in CON, and $\rho_s = 0.15\ D^{-1}$ kg $m^{-3}$ in MODI, where D is the diameter of snow in m. In Section 4, we compare the results of the spherical assumption with those of the non-spherical databases in the Liu simulator (Liu 2008).

**Methodology**

Liu et al. (1995) presented a cloud classification method using CTT of geostationary meteorological satellite (GMS)-4 and a microwave index from scattering and emission channels of the special sensor microwave/imager (SSM/I) over ocean. Matsui et al. (2014)

introduced an evaluation method based on joint diagrams using the CTT (MODIS 11-μm TBs) and PCT89 of AMSR-E to classify cloud types over land following the Liu et al. (1995). The two previous studies use microwave index and PCT89 to distinguish between non-precipitation and precipitation clouds. In this study, we introduce an evaluation method for only precipitation clouds using CTT and PCT89 as a scattering intensity from large ice particles. We discriminate the precipitation clouds by additionally introducing D19 to improve the detection of shallow precipitation clouds than Matsui et al. (2014). This method enables us to investigate high and low precipitation systems using CTT and PCT89 over the ocean. The precipitation areas are identified using the D19 threshold.

Figure 1a shows the joint histogram in terms of the CTT and PCT89 over the domain. There are high frequencies of mixtures of clear sky and cloudy regions with higher CTT and PCT89 than 280 K (Fig. 1a). Figure 1a shows all clouds and does not clearly distinguish between non-precipitation and shallow precipitation. Therefore, we use D19 to focus on the precipitation areas by using a D19 threshold of 50 K; this corresponds to approximately 1 mm hr$^{-1}$ for a typical tropical profile according to Liu and Curry 1996 (in their Fig. 1a). Figure 1b shows the joint histogram of the CTT and PCT89 for the areas whose D19 is lower than 50 K. Using this histogram, we can classify the precipitation clouds into three categories, “warm,” “cold,” and “deep” clouds, using the thresholds of CTT and PCT89. The systems are clearly divided into low and high precipitation clouds by a CTT of 245 K. We refer to clouds with a CTT higher than 245 K as “warm clouds.” For clouds with a CTT less than 245 K, we further divide them into two categories: “cold clouds” for clouds with a PCT89 larger than 250 K and “deep clouds” for clouds with a PCT89 less than 250 K.

Note that the terminology introduced in this study does not precisely follow conventional definitions. “Warm clouds” are mixtures of shallow and cumulus congestus precipitations. According to Machado et al. (1998), the infrared threshold of clouds associated with deep convection is estimated to be 245 K. “Cold clouds” consist of stratiform precipitation in MCSs and shallow/congestus with overlapped cirrus (CTT < 245 K and PCT89 > 250 K). “Deep clouds” (CTT < 245 K and PCT89 < 250 K) are convective and stratiform precipitation of MCSs related to the depression of PCT89 due to snow and graupel.

## Evaluation of NICAM

Using the method introduced in the previous section, we evaluated two simulation results using NICAM. Figure 2 shows the relationship between the averaged D19 and rain rate from the simulations with the two microphysics schemes over the tropical open ocean using the Liu simulator. In these simulations, as in the observations (Liu and Curry 1998), the D19 decreases as the precipitation increases. This is because the emission of precipitating liquid hydrometeors at 18.7 GHz weakens D19 from the polarized ocean surface. D19 has limitations when observing heavy precipitation of over 12 mm hr$^{-1}$ due to the saturation of the microwave radiation. The precipitation rate for a D19 of 50 K is approximately 1 mm hr$^{-1}$. These characteristics linking D19 and the rain rate are consistent with the tropical case with no ice (Liu and Curry 1998). We found that D19 is not sensitive to the microphysics schemes in CON and MODI, even though the D19 of CON reproduces slightly larger averaged precipitation rates than MODI in the D19 regime between 25 K and 60 K. According to Sasaki et al. (2007), the effects from various rain size distributions are small on the simulated brightness temperature at 19 GHz. This lack of sensitivity to cloud microphysics schemes indicates that D19 is a good index of the surface precipitation.

Figure 3 shows the joint histograms of the CTT and PCT89 from simulation results of CON and MODI using the satellite simulators. MODI (Fig. 3b) is closer to the observations (Fig. 1b) than is CON (Fig. 3a); MODI shows structures similar to the observations such as a high frequency of cold clouds and a minimum value of PCT89 near 210 K. Conversely, in the case of CON, the frequency of deep clouds is overestimated and the frequency of cold clouds is underestimated compared to the observations and MODI. Deep clouds in CON have PCT89 much lower than 200 K, which is not seen in the observations or MODI. MODI reproduces a smaller fraction of the deep clouds (5.7%) than is seen in the observations (10.6%). Both of the simulated warm clouds are overestimated compared to the observations.

To understand how MODI improves PCT89, we examined its sensitivity to the size distribution of the ice hydrometeors (Fig. 4). First, only the snow size distribution in MODI was changed from MODI to CON (Fig. 4a). The use of the snow size distribution of CON leads to underestimations of PCT89 compared to the case with the snow size distribution of

MODI. That is, the assumptions in MODI, in which the bimodal size distribution is parameterized by temperatures and the ice water contents are based on Field et al. (2005), lead to an increase in PCT89 compared to that in CON, in which a constant intercept parameter with a negative exponential distribution is assumed. Second, only the graupel size distribution in MODI was exchanged from MODI to CON. The graupel size distribution had a small impact compared to that of the snow size distribution. The joint histogram is more widespread than that of the original MODI. Because the interceptor parameter of graupel in MODI was increased by 100 times compared to that of CON, MODI produces smaller sizes of graupel than does CON. From the above sensitivity, we conclude that the snow size distribution in MODI is the primary factor influencing the improvement in PCT89.

In Figure 5, we compare the above joint histogram of the CTT and PCT89 with that of CTH and PTH as used in RS14. To capture precipitation regions, we focus on the regions with larger surface radar reflectivity, above 20 dBZ; note that a TRMM PR of 21.6 dBZ corresponds to approximately 1 mm hr$^{-1}$ for convective systems (Fig. 9 of Schumacher and Houze 2010). We divided the cold and deep clouds using a PTH of 6 km instead of a PCT89 of 250 K. The two joint histograms capture a similar contrast between CON and MODI. For example, CON shows higher frequencies below 220 K compared to those above a PTH of 12 km (Figs. 3b and 5b) and CON shows a systematic bias, such as at high frequencies with a PTH of 12 km, which corresponds to high frequencies below 220 K that are related to deep clouds. Deep clouds with higher PTH indicate larger sizes of graupel and snow located at higher altitudes. According to RS14, the snow size distribution affects the distribution of PTH. In this study, we found that the size distribution of snow primarily affects the distribution of PCT89.

**Snow shape dependency**

The advantage of using PCT89 is that it is sensitive to ice clouds. Snow has various shapes and affects the scattering properties of high frequency microwave channels like PCT89. Snow shapes have not been fully taken into account in CSRMs and therefore create uncertainties (Geer and Baordo 2014). The previous results are based on a soft sphere assumption (SP) according to Mie calculation with effective dielectric constant from the Maxwell-Gartnett method. The impacts of the non-spherical assumptions of snow are investigated on the normalized probability distribution of PCT89 over the analysis domain using the Liu simulator in off-line (Fig. 6). We used the pre-computed optical properties of five snow shapes, short column (SN1), thin plate (SN4), six bullet rosettes (SN8), dendrite snow (SN10), and aggregate (SN11) according to the discrete dipole approximation (DDA, Purcell and Pennypacker 1973) in a database of microwave single-scattering properties for non-spherical ice particles (Liu 2008; Nowell et al. 2013). The normalized probability distribution of PCT89 shows that MODI reproduces a more realistic distribution compared to the observations than does CON. PCT89 in CON are underestimated compared to MODI and the observations due to the overestimation of scattering from ice particles. In CON, simple structures of snow such as the short column lead to lower PCT89 compared to complicated shapes such six bullet rosettes, dendrite snow, and aggregate. Dendrite snow has a similar distribution to that of the soft sphere assumption in CON and MODI. The impact of the non-spherical assumption is different for CON and MODI. MODI experiences a smaller impact from the snow shapes than does CON because the size of the snow is smaller in MODI than in CON. The non-spherical assumption has a strong impact on the large size snow. The PCT89 distribution pattern more strongly depends on the size distribution of the snow than does the non-spherical assumptions.

## Summary

We present an evaluation method for precipitation clouds in CSRMs using 11-μm TB from a geostationary satellite and PCT89 and D19 from a passive microwave satellite over the ocean using satellite simulators based on Liu et al. (1995) and Matsui et al. (2014). This method can investigate precipitation clouds detected by D19 using two indices related to the CTT and PCT89, which represent the cloud-top height and scattering intensities from large ice particles, respectively. This method enables us to quantitatively evaluate shallow and deep precipitation clouds in simulations by comparing them to their observational counterparts.

Two NICAM simulations using different cloud microphysics schemes were evaluated over the tropical open ocean. We found that the simulation results with the modified cloud microphysics scheme (MODI) developed by RS14 closer to the observations than the original scheme (CON). We found that the improvement of PCT89 in RS14 is primarily derived from the change in the size distribution of the snow rather than that of the graupel in the cloud microphysics scheme.

The new method presented in this study shows similar results to those for the TRMM-based analysis in RS14. The passive microwave satellite has limitations when distinguishing shallow and congestus precipitation compared to PTH from TRMM PR. The distribution of the joint histograms of PTH and CTT clearly shows three modes: shallow clouds (PTH < 4 km and CTT < 273 K), congestus (4 < PTH < 6 km and CTT > 245 K), and deep clouds (PTH > 6 km and CTT < 245 K). The advantage of the joint histogram with CTT and PTH is that it can distinguish shallow and congestus clouds clearly using a PTH of 4 km and a CTT of 245 K (Fig. 5a). TRMM PR has a finer horizontal resolution (5 km) for detecting precipitation regions compared to D19 (approximately 18 km). However, passive microwave satellites are abundant, e.g., AQUA, TRMM, and Global Precipitation Measurement (GPM), and the swath that is covered is approximately 1450 km compared to the 247 km covered by TRMM PR. This means that the present method is more appropriate when collecting sampling data with wider coverage than those of TRMM PR.

In addition to the wider swath coverage, passive microwave satellite sensors are sensitive to ice cloud properties. We tested non-spherical assumptions for snow compared to the Mie theory using a database of optical properties from DDA with a satellite simulator. The size distribution of snow had a strong impact on the depression of PCT89 compared to the non-spherical assumptions. The impact of the non-spherical assumption on the distribution of PCT89 depends on the parameterization of the snow size distribution in the cloud microphysics schemes.

Many more satellites carry passive microwave sensors than carry precipitation radar sensors. That means that more sampling data are available from passive microwave sensors. Therefore, it is possible to evaluate the simulations of CSRMs with a smaller domain and shorter integration time than is possible with a method using active microwave sensors. In addition, it should be useful to investigate quantitatively warm and deep precipitation clouds in the different environmental conditions such as sea surface temperatures and, more importantly, ice cloud properties, which are one of the most uncertain parts of CSRMs, should be evaluated and improved.

## Acknowledgments

The authors are grateful to anonymous reviewers for their constructive comments. We thank Professor G. Liu of Florida University and Professor H. Masunaga of Nagoya University for use of satellite simulators and their helpful discussions. TRMM data and AMSR-E were obtained from NASA and the Japan Aerospace Exploration Agency (JAXA). An analysis was done on the NEC SX supercomputer at the Center for Global Environmental Research of the National Institute for Environmental Studies. This research

Fig. 1

was supported by the EarthCARE Program of the Earth Observation Research Center of JAXA.

## References

Ashcroft, P. and F. J. Wentz. 2013. *AMSR-E/Aqua L2A Global Swath Spatially-Resampled Brightness Temperatures*. Version 3. Boulder, Colorado USA: NASA National Snow and Ice Data Center Distributed Active Archive Center. http://dx.doi.org/10.5067/AMSR-E/AE_L2A.003.

Bohren, C. F., and L. J. Battan, 1982: Radar backscattering of microwaves by spongy ice spheres. *J. Atmos. Sci.*, **39,** 2623–2628.

Eito, H., and K. Aonashi, 2009: Verification of hydrometeor properties simulated by a cloud-resolving model using a passive microwave satellite and ground-based radar observations for a rainfall system associated with the Baiu Front. *J. Meteor. Soc. Japan*, **87A,** 425–446.

Field, P. R., R. J. Hogan, P. R. A. Brown, A. J. Illingworth, T. W. Choularton, and R. J. Cotton, 2005: Parametrization of ice-particle size distributions for mid-latitude stratiform cloud. *Q. J. R. Meteorol. Soc.*, **131,** 1997–2017.

Geer, A. J., and F. Baordo, 2014: Improved scattering radiative transfer for frozen hydrometeors at microwave frequencies. *Atmos Meas Tech*, **7,** 1839–1860.

Han, M., S. A. Braun, W. S. Olson, P. O. G. Persson, and J.-W. Bao, 2010: Application of TRMM PR and TMI measurements to assess cloud microphysical schemes in the MM5 for a winter storm. *J. Appl. Meteorol*, **49,** 1129–1148.

Hashino, T., M. Satoh, Y. Hagihara, T. Kubota, T. Matsui, T. Nasuno, and H. Okamoto 2013: Evaluating cloud microphysics from NICAM against CloudSat and CALIPSO. *J. Geophys. Res.: Atmos.*, **118**, 7273–7292.

Kidd, C., 1998: On rainfall retrieval using polarization-corrected temperatures. *Int. J. Remote Sens.*, **19,** 981-996.

Liu, G. S., J. A. Curry, and R. S. Sheu, 1995: Classification of Clouds over the Western Equatorial Pacific-Ocean Using Combined Infrared and Microwave Satellite Data. *J. Geophys. Res.: Atmos.*, **100,** 13811-13826.

Liu, G. S., and J. A. Curry, 1998: An investigation of the relationship between emission and scattering signals in SSM/I data. *J. Atmos. Sci.*, **55,** 1628–1643.

Liu, G. S., 1998: A fast and accurate model for microwave radiance calculations. *J. Meteor. Soc. Japan,* **76**, 335–343.

Liu, 2008: A database of microwave single-scattering properties for nonspherical ice particles. *Bull. Amer. Meteorol. Soc.*, **89**, 1563–1570.

Masunaga, H., and C. D. Kummerow, 2005: Combined radar and radiometer analysis of precipitation profiles for a parametric retrieval algorithm. *J Atmos Ocean Tech*, **22,** 909-929.

Masunaga, H., and C. D. Kummerow, 2006: Observations of tropical precipitating clouds ranging from shallow to deep convective systems. *Geophys. Res. Lett.*, **33**.

Masunaga, H., T. Matsui, W.-K. Tao, A. Y. Hou, C. D. Kummerow, T. Nakajima, P. Baeur, W. S. Olson, M. Sekiguchi, and T. Y. Nakajima, 2010: Satellite data simulator unit: a multisensor, multispectral satellite simulator package. *Bull. Amer. Meteorol. Soc.*, **91,** 1625–1632.

Matsui, T., X. Zeng, W.-K. Tao, H. Masunaga, W. S. Olson, and S. Lang, 2009: Evaluation of long-term cloud-resolving model simulations using satellite radiance observations and multifrequency satellite simulators. *J. Atmos. Oceanic Technol.*, **26,** 1261–1274.

Matsui, T., and Coauthors, 2014: Introducing multisensor satellite radiance-based evaluation for regional Earth System modeling. *J Geophys Res-Atmos*, **119**.

Matsui, T., J. D. Chern, W. K. Tao, S. Lang, M. Satoh, T. Hashino, and T. Kubota, 2016: On the land-ocean contrast of tropical convection and microphysics statistics derived from TRMM satellite signals and global storm-resolving models. *J Hydrometeorol*, **17,** 1425–1445.

Maxwell Garnett, 1904: Colours in Metal Glasses and Metal Films, *Philos. Trans. R. Soc. London Ser. A*, **203,** 385–420.

Nowell, H., G. S. Liu, and R. Honeyager, 2013: Modeling the microwave single-scattering properties of aggregate snowflakes. *J Geophys Res-Atmos*, **118,** 7873-7885.

Purcell, E. M., and C. R. Pennypacker, 1973: Scattering and absorption of light by nonspherical dielectric grains. *The Astrophysical Journal*, **186,** 705–714.

Roh, W., and M. Satoh, 2014: Evaluation of precipitating hydrometeor parameterizations in a single-moment bulk microphysics scheme for deep convective systems over the tropical Central Pacific. *J. Atmos, Sci.*, **71,** 2654–2673.

Roh, W., M. Satoh, and T. Nasuno, 2017: Improvement of a cloud microphysics scheme for a global Nonhydrostatic Model Using TRMM and a Satellite Simulator. *J. Atmos, Sci*, **74,** 167–184.

Sasaki, H., S. Shige, and K. Okamoto (2007), Improvements of brightness temperature simulations for validation of TRMM rainfall products (in Japanese), *J. Remote Sens. Soc. Jpn.*, **27**, 153–166.

Satoh, M., T. Matsuno, H. Tomita, H. Miura, T. Nasuno, and S. Iga, 2008: Nonhydrostatic icosahedral atmospheric model (NICAM) for global cloud resolving simulations. *J. Comput. Phys.*, **227,** 3486–3514.

Satoh, M., and Y. Matsuda, 2009: Statistics on high-cloud areas and their sensitivities to cloud microphysics using single-cloud experiments. *J. Atmos, Sci.*, **66,** 2659–2677.

Satoh, M., T. Inoue, and H. Miura, 2010: Evaluations of cloud properties of global and local cloud system resolving models using CALIPSO and CloudSat simulators. *J. Geophys. Res.: Atmos.*, **115**.

Satoh, M., Tomita, H., Yashiro, H., Miura, H., Kodama, C., Seiki, T., Noda, A. T., Yamada, Y., Goto, D., Sawada, M., Miyoshi, T., Niwa, Y., Hara, M., Ohno, Y., Iga, S., Arakawa, T., Inoue, T., Kubokawa, H. 2014: The Non-hydrostatic Icosahedral Atmospheric Model: Description and development. *Progress in Earth and Planetary Science*. **1**, 18.

Schumacher, C., and R. A. Houze. Jr., 2000: Comparison of radar data from the TRMM satellite and Kwajalein oceanic validation site. *J Appl Meteorol*, **39,** 2151–2164.

Spencer, R. W., H. M. Goodman, and R. E. Hood, 1989: Precipitation retrieval over land and ocean with the SSM/I: Identification and characteristics of the scattering signal. *J Atmos Ocean Tech*, **6,** 254–273.

Tomita, H., and M. Satoh, 2004: A new dynamical framework of nonhydrostatic global model using the icosahedral grid. *Fluid Dyn Res*, **34,** 357–400.

Tomita, H., 2008a: New microphysical schemes with five and six categories by diagnostic generation of cloud ice. *J. Meteorol. Soc. Jpn.*, **86,** 121–142.

Tomita, H., 2008b: A stretched icosahedral grid by a new grid transformation. *J. Meteorol.l Soc. Jpn.*, **86,** 107–119.

## List of Figures

Fig. 1  Joint histograms between PCT89 and CTT from AMSR-E and MTSAT over (a) the tropical open ocean and (b) only the precipitation regions defined by the threshold of a

D19 of 50 K. The unit of the color bar is % $K^{-1}$ $K^{-1}$.

Fig. 2 Plot of D19 and the averaged rain rate over the tropical open ocean in CON and MODI.

Fig. 3 Joint histograms of PCT89 and CTT over the tropical open ocean with D19 lower than 50 K in (a) CON and (b) MODI. The unit of the color bar is % $K^{-1}$ $K^{-1}$.

Fig. 4 (a) Same as Fig. 3b except for the snow size distribution of CON, and (b) same as Fig. 3b except for the graupel size distribution of CON. The unit of the color bar is % $K^{-1}$ $K^{-1}$.

Fig. 5 Joint histograms of PTH and CTT over the tropical open ocean from (a) TRMM, (b) CON, and (c) MODI. The unit of the color bar is % $km^{-1}$ $K^{-1}$.

Fig. 6 The normalized probability distributions of PCT89 over the analysis domain with various shape assumptions of snow for (a) CON and (b) MODI.

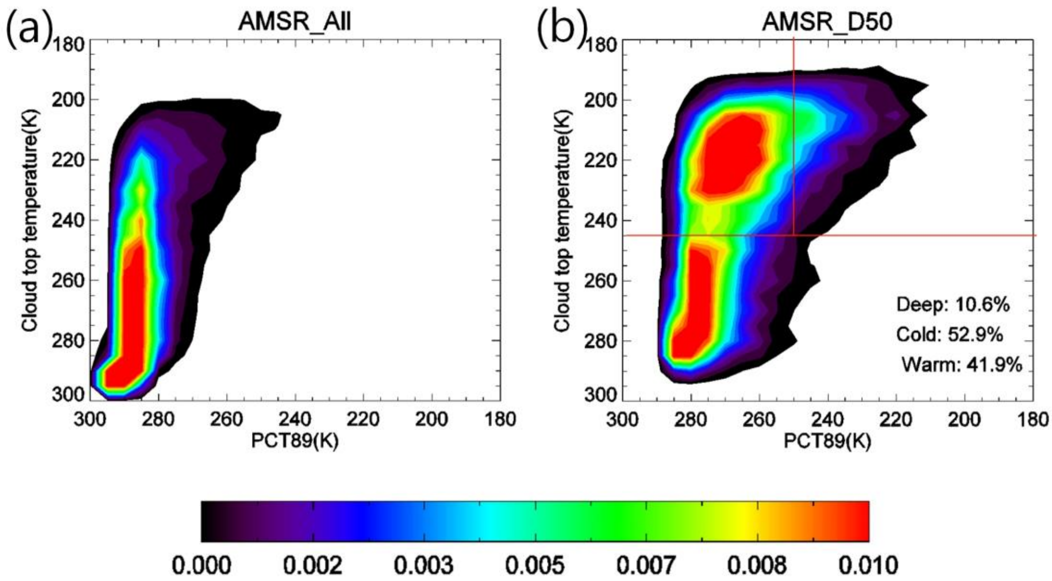


Fig. 1 Joint histograms between PCT89 and CTT from AMSR-E and MTSAT over (a) the tropical open ocean and (b) only the precipitation regions defined by the threshold of a D19 of 50 K. The unit of the color bar is % $K^{-1}$ $K^{-1}$.

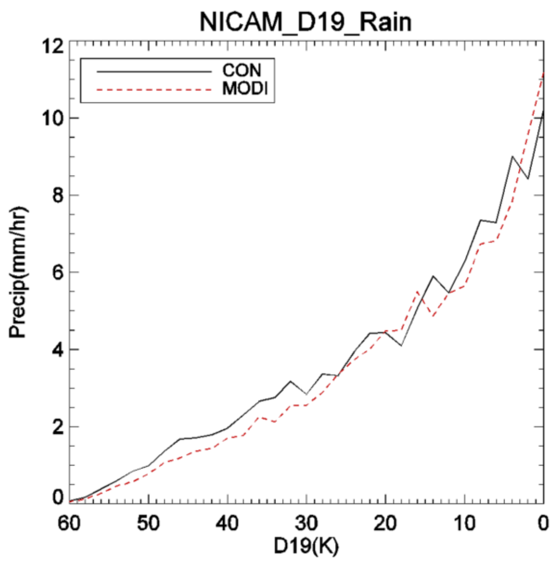


Fig. 2 Plot of D19 and the averaged rain rate over the tropical open ocean in CON and MODI.

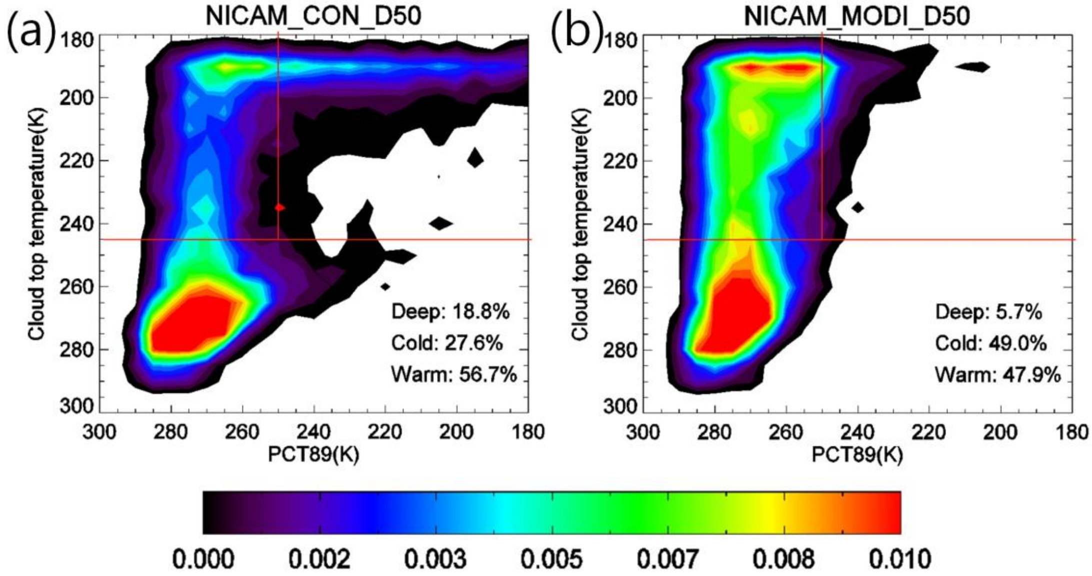


Fig. 3 Joint histograms of PCT89 and CTT over the tropical open ocean with D19 lower than 50 K in (a) CON and (b) MODI. The unit of the color bar is % $K^{-1}$ $K^{-1}$.

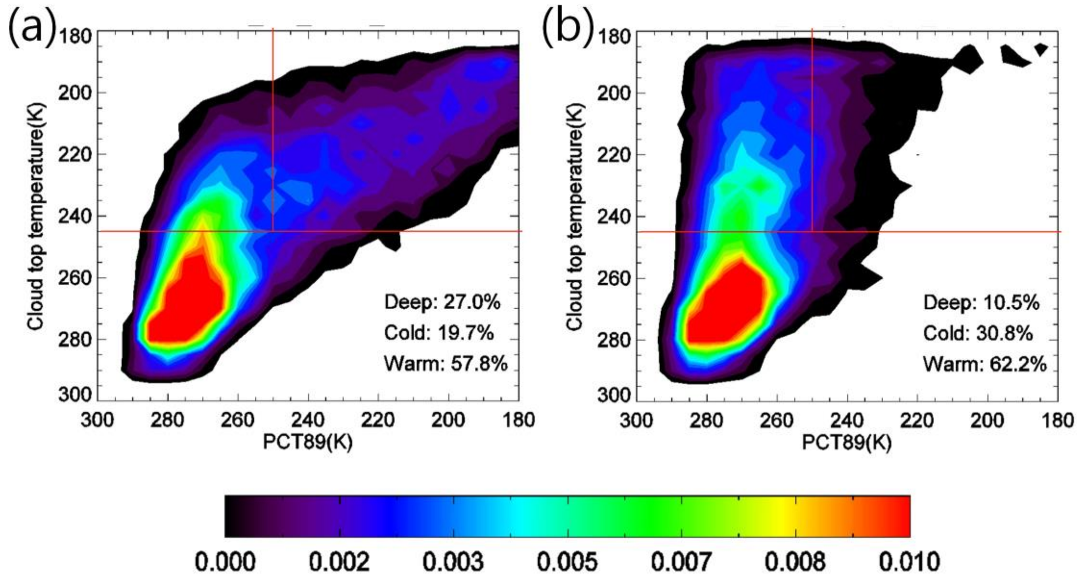


Fig. 4 (a) Same as Fig. 3b except for the snow size distribution of CON, and (b) same as Fig. 3b except for the graupel size distribution of CON. The unit of the color bar is % $K^{-1}$ $K^{-1}$.

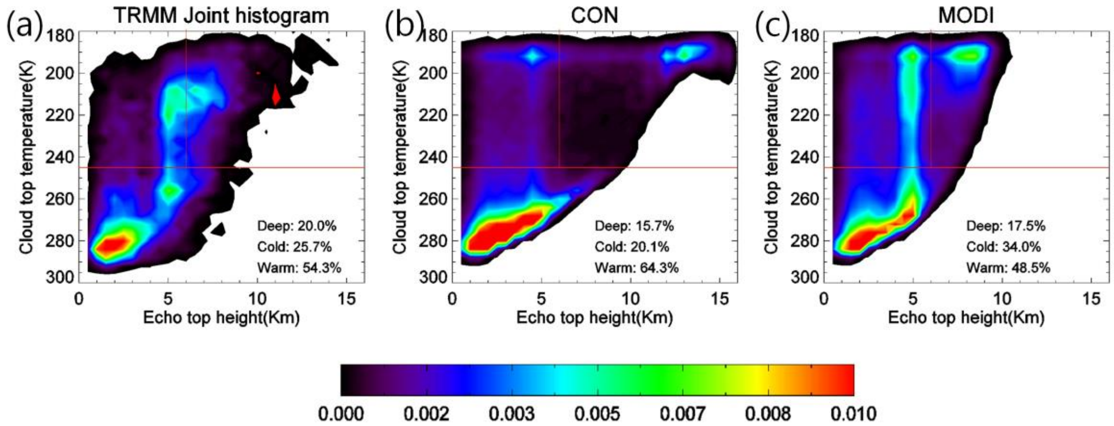


Fig. 5 Joint histograms of PTH and CTT over the tropical open ocean from (a) TRMM, (b) CON, and (c) MODI. The unit of the color bar is % km$^{-1}$ K$^{-1}$.

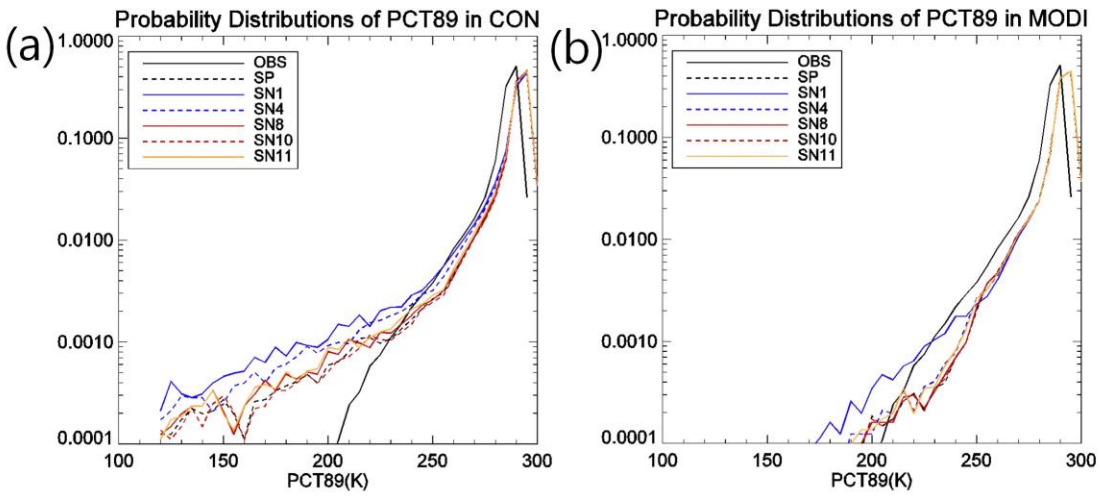


Fig. 6 The normalized probability distributions of PCT89 over the analysis domain with various shape assumptions of snow for (a) CON and (b) MODI.